International Journal of Pure and Applied Physics.
ISSN 0973-1776 Volume 21, Number 1 (2025), pp. 1-8

http://www.ripublication.com

Electron Momentum Density, Fermi Surface Mapping, and Electronic State Classification in AgZn Alloy

A S Hamid[1,2]

[1] *Department of Physics, College of Science, Qassim University, 51452, Buraydah, Almolaydah, Saudi Arabia*

[2] *Department of Physics, Faculty of Science, Helwan University, Helwan 12812 Cairo, Egypt*

Abstract

We report a detailed investigation of the electron momentum density and Fermi surface topology of equiatomic β′-AgZn, from two-dimensional angular correlation of positron annihilation radiation (2D-ACAR) measurements. Using a Fourier-based reconstruction algorithm, the three-dimensional momentum density was reconstructed from multiple 2D-ACAR projections and subsequently folded into the first Brillouin zone using the Lock–Crisp–West (LCW) procedure. The resulting LCW map provides direct insight into the Fermi surface (FS) of AgZn. The results show that the Fermi surface of AgZn, as revealed by 2D-ACAR, consists of a prominent electron sheet in the second band that extends to the Brillouin zone faces along <100> directions, and a characteristic "hole octahedron" in the first band.

1. Introduction

Ordered β'-AgZn (equiatomic silver–zinc) is a CsCl-type (B2 structure) intermetallic alloy that has attracted interest as a Hume-Rothery alloy with an atypical Fermi surface due to its *sp*-electron valence structure (see Figure 1). In β'-AgZn, each formula unit contributes three valence electrons (nominally Ag *5s* and Zn *4s*), resulting in partially filled conduction bands and a complex Fermi surface despite the simple cubic crystal symmetry. Prior studies using de Haas–van Alphen (dHvA) oscillations identified distinctive Fermi surface features of β'-AgZn, notably a hole octahedron in the first band and a triangular hole in the second band [1-6]. These features were found to be in good agreement with earlier band structure calculations [7], which showed that β'-AgZn's Fermi surface closely resembles that of isoelectronic β'-CuZn and related β-brass alloys [8, 9]. In particular, the theoretical work indicated that the Ag *4d* and Zn

3d bands lie far below the Fermi energy and do not participate in bonding, whereas the valence *s*-band splits into a fully occupied bonding state and a partially occupied anti-bonding state [10- 12]. This electronic structure (with one more valence electron than a simple noble metal) produces a Fermi surface that deviates from a single nearly-free-electron sphere and contains both electron and hole pockets.

The experimental data were collected using 2D angular correlation of annihilation radiation (ACAR) spectroscopy. The electron momentum density ***ρ(p)*** was reconstructed employing a directed Fourier transformation-based technique [13]. Fermi surface (FS) topologies were determined through the Lock–Crisp–West (LCW) folding procedure [14]. FS sheet dimensions were derived by analysing the maximum gradient of the momentum density distribution in wave vector space and subsequently compared with theoretical calculations. This paper is structured as follows: Section 2 briefly describes the experimental approach and data analysis procedures; Section 3 discusses the results concerning the electronic structure, electron momentum density ***ρ(p)***, and FS topologies; finally, conclusions drawn from the results are presented.

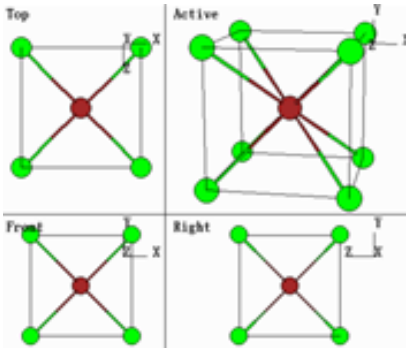

Figure 1 Crystal structure of β-AgZn (B2 type). Silver (Ag) atoms occupy the cube corners (positions: 0,0,0), and zinc (Zn) atoms occupy the body-centered positions (positions: ½,½,½). Each atom is coordinated by eight nearest neighbours of the opposite type, forming a highly ordered cubic arrangement (CsCl structure type).

2. Experimental Details

The sample used in the present experiments is single crystal of AgZn was chemically etched with a solution of HNO_3 and HF and annealed in vacuum for 20 hours. In view of the concentration of defects, The measured lifetime spectra were analysed by assuming one annihilation mode. The value of the lifetime component shows single component beside the source components [15]. The sample was measured using 2D-ACAR experiments discussed elsewhere [13]. The total counts of each spectrum were 2.0×10^7 counts. The measurements were carried out for ten successive orientations by rotating the sample out <001> axis from <100> to <110> in increments of 5º. This shows accumulation of ***ρ(p)*** about $1x10^8$ in the ten projections. The estimation of the experimental resolution was calculated from, mainly, three

sources; the angular resolution of the detectors; the smearing of the thermal motion of positron; and the smearing due to finite area of annihilation. This shows experimental resolution about 0.75×10^{-3} m_oc, 0.24×10^{-3} m_oc and 0.63×10^{-3} m_oc, respectively [16]. As a results, the overall angular resolution of the system was (1.2×10^{-3} m_oc), where m_o is the mass of the electron and c is the speed of light. This estimation was verified by measuring the full width at half maximum FWHM of a single crystal of quartz [17]. The spectra were reconstructed using reconstruction technique based on Fourier transform [18]. The method includes interpolation in the Fourier space, and inverse Fourier transformation followed by basic Fourier projection theorem. The experimental accuracy was determined from the comparison of the integrated spectrum before the reconstruction and the reconstructed spectrum, in the same direction [19]. It showed uncertainty in the reconstructed spectra and consequently in the dimensions of the FS about 0.02 a.u in all directions (10^{-3} m_oc = 0.137 a.u) [19].

3. Results and Discussion

Momentum Density Distribution from 2D-ACAR

Figure 2 shows a representative two-dimensional slice of the momentum density in the p_z=0 plane (a plane containing the <100> directions. Several features of the momentum density are evident. First, the distribution is centred around ρ(p)=0 but notably is not maximum at p=0. Instead, ***ρ(p)*** exhibits a shallow minimum at p=0, and increases to a broad maximum at finite momentum at 0.5 a.u. (edges of the central region in Fig. 2, p_z=0). This non-monotonic behaviour is a hallmark of an electron gas with a Fermi cut-off: in an ideal Fermi gas at T=0^o, the momentum distribution n(p) is unity for $p< p_F$ and zero for $p>p_F$, leading to an integrated momentum density that is flat inside the Fermi sphere and then drops. In the experimental ***ρ(p)***, which is effectively the occupation weighted by positron wavefunction overlap, this appears as a slight depletion at low ***p*** and an enhancement just below the Fermi momentum. In AgZn, the enhancement of ***ρ(p)*** at $\boldsymbol{p_F}$ is relatively small (on the order of 5–10%), consistent with a moderate contrast in occupation (the occupancy in momentum space does not drop sharply from 1 to 0 because of positron filtering and finite resolution).

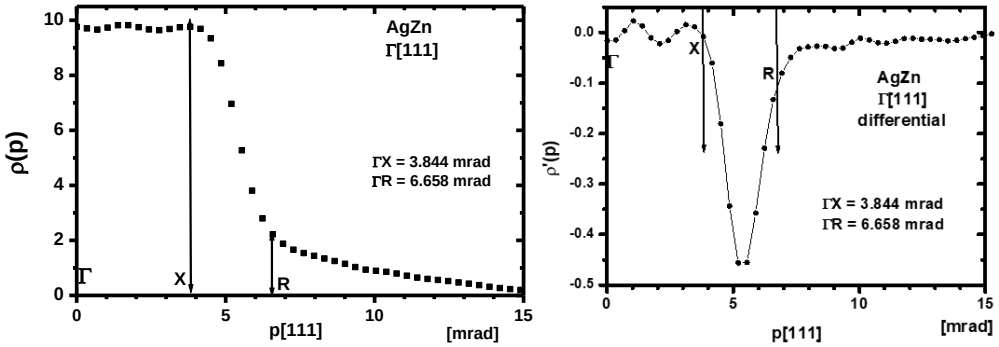

Figure 2: Measured 2D momentum density distribution in AgZn. High intensity corresponds to higher electron momentum density, and low intensity to lower density (arbitrary units). The data are symmetric about the centre as expected. b) the maximum gradient value of ρ' (P).

Secondly, the momentum density is highly isotropic and cubic-symmetric, as expected for a cubic crystal. No strong anisotropies are visible in Fig. 2; the contours of constant ***ρ(p)*** are nearly circular (or square, following the symmetry) about the centre. This suggests that the Fermi surface is fairly spherical or only weakly modulated by the lattice potential. Nonetheless, closer inspection (and analysis of other slices) reveals a subtle anisotropy: ***ρ(p)*** is slightly higher along the <100> axes than along <110> directions. For example, along the $\boldsymbol{p_x}$ axis (horizontal direction through the center of Fig. 1), the momentum density falls off a bit more slowly than along the ***px***=***py*** diagonal. This is evidence of the Fermi surface not being a perfect sphere – the occupation extends farther out in the <100> directions than in the <110> directions. Such anisotropy is consistent with the expected cubic distortions of the Fermi surface in the ***B2*** structure (discussed below). Apart from these Fermi surface-related anisotropies, no signatures of discontinuities are directly visible in the raw ***ρ(p)***; the 2D-ACAR data is too smeared by resolution to directly show a sharp break at $\boldsymbol{p_F}$. Therefore, we turn to the LCW folding analysis to more directly visualize the Fermi surface.

Fermi Surface from LCW Folding of ACAR Data

Applying the LCW folding to the 3D momentum density, we obtained the electron occupancy distribution ***n(k)*** in the first Brillouin zone of the B2 (bcc) lattice. In an ideal scenario, ***n(k)*** would equal the number of occupied bands (2 or 3 in this case) for ***n(k)*** inside the Fermi volume and drop to a lower value for ***k*** outside the Fermi volume. In practice, our folded distribution shows occupancy values close to 3 electrons per cell in most regions of ***k***-space, with slight deviations (0.25) near the Fermi surface. The Fermi surface can thus be visualized by plotting the iso-surface (or contour) where ***n(k)*** transitions between high and low values. **Figure 3** presents the LCW-folded momentum density in a representative plane ($\boldsymbol{k_z=0}$ plane), with the Fermi surface contour indicated. From Fig. 3, we clearly discern the main features of the AgZn Fermi surface. The most prominent feature is the large electron sheet in the second band,

centered on Γ and extending along the <100> directions. In the folded map, this corresponds to the red regions bulging towards the Brillouin zone faces (midpoints of the edges in Fig. 3). We see that along the [100] direction (toward the middle of the right edge in Fig. 3), the occupancy remains high (near 3) all the way to the zone boundary, indicating that the second band is occupied up to the zone face. The black contour labelled as FS cuts through these edge centres, confirming that the Fermi surface intersects the zone boundary at the ***H*** points (face centres). In contrast, along the [110] diagonal direction (towards the corners of the square in Fig. 3), the occupancy falls off more rapidly (blue regions at the corners). By the zone corner (P) point, at the corner of the square) the occupancy is low (approximately 2.74, meaning essentially only the bonding band is filled and the antibonding band is empty). This means the second-band Fermi surface does not reach the zone corners; instead, there is a hole pocket there. The LCW map thus clearly shows the presence of triangular hole pockets at the Brillouin zone corners (P points). These appear as the blue triangular regions in Fig. 3 at the corners, bounded by the FS contour. This triangular hole in the second band is precisely the feature identified by dHvA as a "triangular hole orbit". Our 2D-ACAR results confirm its existence and size.

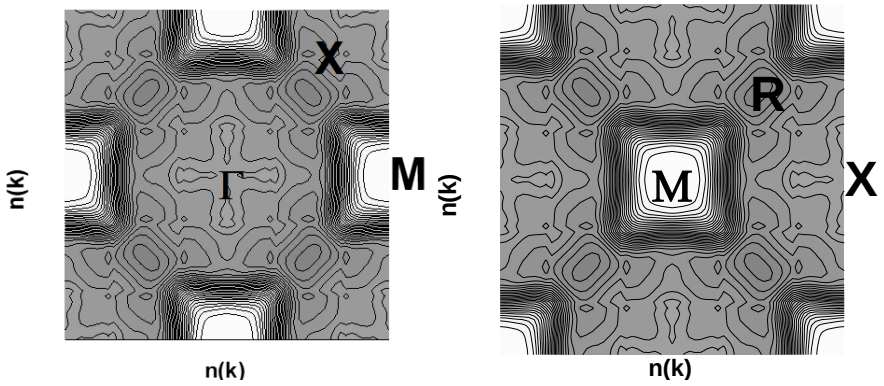

Figure 3: LCW-Folded Electron Momentum Density In The First Brillouin Zone (In The Kz=0 Plane). Red Regions Indicate Higher Ocupancy (Close To 3 Electrons/Cell), Blue Regions Indicate Lower Occupancy (Below 3). The Black Line Denotes The Fermi Surface Contour (Where The Occupancy Drops Halfway). The Brillouin Zone Boundary In Theis Plane Is At The Midpoint Of Each Edge.

Additionally, the LCW data provides evidence of the first-band hole octahedron. In the occupancy plot (Fig. 3), the very centre Γ is slightly blue-tinted relative to the immediate surroundings, meaning the occupancy at is a bit below 3. This indicates that even at Γ the second band is not fully occupied – a subtle sign that the first band might have already dropped below $\boldsymbol{E_F}$ in some directions, creating a small hole. The first-band Fermi surface (if any) would be a hole-type surface inside the first Brillouin zone. In a bcc zone, a hole octahedron would be centered at Γ and oriented such that it touches the zone boundaries along the <100> directions ***N*** points. While the LCW map's contrast is limited, we do observe a slight

depression in occupancy near the ***N*** points (e.g., along the midpoints of the top/bottom edges in Fig. 3, the occupancy is a few percent lower than 3). This suggests a tiny first-band hole "octahedron" feature. In dHvA experiments, such a hole octahedron in AgZn was indeed detected and its shape determined by Fourier inversion of orbits. Our positron data is consistent with this, though the signal is weak because the volume of the hole is small (the first band is almost completely filled).

Overall, the Fermi surface of AgZn as revealed by the 2D-ACAR and LCW analysis comprises: (i) a large central electron surface (second band) which is roughly cubic-rounded in shape, bulging out to the zone faces, and (ii) additional hole pockets: small octahedral holes at Γ (first band) and prominent triangular holes at the zone corners (second band). This topology is in excellent qualitative agreement with the Fermi surface predicted by DFT band structure[20].

Comparison of Fermi Surface Dimensions

Table 1 summarizes key Fermi surface characteristics of AgZn as obtained from our 2D-ACAR (LCW) analysis, and as reported by dHvA measurements [1] and by band-structure calculations [7]. We list the approximate Fermi radii or extremal cross-sectional dimensions along representative directions for the major FS sheets. Uncertainties in the ACAR values are on the order of $\Delta = 0.05 \times (2\pi/a)$ due to finite resolution. Good agreement between 2D-ACAR and other data is quite good.

Table 1. Comparison of Fermi surface dimensions in AgZn derived from 2D-ACAR (this work) versus de Haas–van Alphen (dHvA) experiments and DFT band calculations.

FS Sheet	FS Feature direction	2D-ACAR (this work)	dHvA [1]	DFT [7]
2nd band	electron radius [100]	~0.95 Γ–H	~0.95 of Γ–H	~1.00 of Γ–H
2nd band	electron radius [110]	~0 (no extension to corner)	~0 (triangular hole orbit present)	~0 (FS open at P, hole present)
1st band	hole octa radius [111] (Γ–N)	0.10–0.15 of Γ–N	~0.15 of Γ–N	~0.12 of Γ–N

(Note: Γ–H is half the edge of the bcc Brillouin zone; Γ–P is the zone diagonal to corner; Γ–N is half the distance to a face center (N point).)

Conclusion

In summary, we have performed a comprehensive study of the electron momentum distribution and Fermi surface of β′-AgZn using 2D positron annihilation spectroscopy. The reconstructed

3D momentum density from 2D-ACAR experiments, when folded into the first Brillouin zone, reveals the Fermi surface topology in excellent agreement with theoretical predictions and previous dHvA results. The AgZn Fermi surface consists of a large cubic-like electron sheet (second band, antibonding ***s***-states) that reaches the Brillouin zone faces along <100>, in addition to characteristic hole pockets: a small octahedral hole around $\boldsymbol{\Gamma}$ (first band, bonding ***s***-state) and triangular holes at the zone corners (in the second band). These features reflect the underlying band structure in which AgZn's valence electrons occupy a filled bonding band and a half-filled antibonding band. The Ag–Zn interaction thus leads to a Fermi surface more complex than a single sphere, featuring both electron-rich regions and electron-depleted regions in ***k***-space.

Our DFT band structure and DOS calculations corroborate the experimental findings, showing that Ag ***5s***–Zn ***4s*** hybridization produces bonding vs. antibonding splitting, with the Fermi level cutting through the antibonding band. The Ag ***4d*** and Zn ***3d*** states remain well below $\boldsymbol{E_F}$ and do not contribute to the Fermi surface (non-bonding core-like states). The momentum density analysis further highlights that positron annihilation is sensitive to subtle occupancy variations: we observed a momentum density minimum at $\boldsymbol{p}=0$ and slight anisotropies consistent with the Fermi surface breaks.

This work demonstrates the effectiveness of 2D-ACAR plus LCW folding in mapping Fermi surfaces in multicomponent alloys. In AgZn, the method successfully identified the same Fermi surface pieces that had been inferred from dHvA, and provided a direct real-space picture of electron momentum sharing between bonding and antibonding states. The consistency between 2D-ACAR, dHvA, and DFT builds confidence in our understanding of the electronic structure of AgZn. Going forward, similar positron annihilation studies on related B2-phase alloys (e.g. AgMg, CuZn, PdIn) could provide further insight into the evolution of Fermi surface features with electron count and potential subtle correlation effects beyond DFT.

References

[1] A.E. Dunsworth and J. P. Jan, The de Haas-van Alphen effect and Fermi surface of the ordered alloy β′-AgZn, Published: October 1973,Volume 13, pages 53–58, (1973)

[2] J.-P. Jan, W. B. Pearson, and Y. Saito,Proc. Roy. Soc. (London)A297, 275 (1967).

[3] J.-P. Jan and C. M. Perrott,J. Low Temp. Phys. 8, 195 (1972).

[4] H. L. Skriver, The Electronic Structure of the Ordered Brass Alloys β′-CuZn and β′-AgZn as Determined by the APW Method, Thesis, Report No. 15, Danmarks Tekniske Højskoele, Lyngby, Denmark, January 1973.

[5] H. L. Skriver,Solid State Commun.11, 1355 (1972).

[6] H. L. Skriver, to be published, F. M. Mueller,Phys. Rev. 148, 636 (1966).

[7] Nihat Arıkana, Ülkü Bayhanb, First-principles study of electronic and dynamic properties of AgMg and AgZn, Solid State Communications,

[8] L. Charrin, A. Combe, G. Moya, Calorimetric study of internal oxidation in Ag-Mg alloys, Materials Science, Materials Science, Acta Metallurgica, DOI:10.1016/0001-6160(81)90041, 1981

[9] P. Verma et al., J. Mater. Sci. Technol., (2004)
[10] B.C. Prorok et al., IEEE Trans. Appl. Supercond., (2000)
[11] D. Sing et al. , Pramana J. Phys., (2009)
[12] M. Kamal et al., J. Mater. Sci. Mater. Electron, (2008)
[13] A. S. Hamid, Sol. Stat. Commu, 147, 490 (2008)
[14] D G Loucks, V H C Crisp and R N West J. Phys. F3. 561 (1973)
[15] A. S Hamid, A. Uedono, T. Chikyow, K. Uwe, K. Mochizuki and S. Kawaminami, Phys. Stat. Soli (a) 203, 300 (2006).
[16] J P Peng, K G Lynn, M T Umlor, D J Keeble and D R Harshman, Phys. Rev. B 50. 15 (1994).
[17] R. Suzuki and M. Osawa, S. Tanigawa, M. Matsumoto, and N. Shiotani, J. Phys. Soc. Jpn, vol. 58, 3251(1989).
[18] Wu. N, Losovyj. Ya. B., David Wisbey, Belashchenko.K, Manno. M , Wang. L, Leighton C, and Dowben1.P. A, Journal of Physics: Condensed Matter 19, 156224 (2007).
[19] A. S Hamid, A Uedono, Zs. Major, T. D. Haynes, J. Laverock, M. A. Alam, S. B. Dugdale and D. Fort, Phys. Rev. B 84, 235107 (2011).
[20] A E Dunsworth, J -P Jan, H L Skriver, De Haas-van Alphen effect and LMTO bandstructure of Al2Cu, Journal of Physics F Metal Physics,
[21] D. B. Tung, T. J. Watson-Yang, and J. Callaway, *Phys. Rev. B* **4**, 3338 (1971). (Electronic structure of ordered β-brass CuZn, for comparison)
[22] P. E. Mijnarends, in *Positron Annihilation*, eds. P. G. Coleman et al. (Academic Press, 1982), p. 25. (Discussion of ACAR and LCW folding technique)